Contract No.:

This manuscript has been authored by Savannah River Nuclear Solutions (SRNS), LLC under Contract No. DE-AC09-08SR22470 with the U.S. Department of Energy (DOE) Office of Environmental Management (EM).

Disclaimer:

A novel approach to modeling biomass pyrolysis in a fluidized bed reactor

Benjamin Caudle[†], Maximilian B. Gorensek[,‡], Chau-Chyun Chen[†]*

[†]Department of Chemical Engineering, Texas Tech University, P.O. Box 43121, Lubbock, Texas 79409-3121, United States

[‡]Advanced Modeling, Simulation, and Analytics, Savannah River National Laboratory, Savannah River Site, 703-41A/225, Aiken, South Carolina 29808, United States

[*]Phone: +1 803 725-1314; Email: maximilian.gorensek@srnl.doe.gov

ABSTRACT: A novel approach to simulating biomass pyrolysis in a fluidized bed of mostly inert material is presented. The bed is assumed to be externally heated, although simulation of autothermal operation with partial oxidation of the products is a future objective. Combining pyrolysis reactions kinetics developed by the CRECK Modeling Group and a previously published component properties model, material and energy balances are closed by tracking the residence time of biomass particles without regard for their exact spatial distribution. The model is used to simulate a pilot-scale fluidized bed pyrolysis process being developed at Iowa State University and model predictions are compared with experimental results for red oak and corn stover feedstocks. The results are in general agreement, with the model typically predicting more non-condensable gas and less low-boiling liquid products. The differences are ascribed to the

limitations of the kinetics model. This model provides a rigorous energy balance for fluidized bed pyrolysis processes that can be incorporated into commercial flowsheet models with the capacity for future addition of partial oxidation reactions and implementation of improved kinetics models.

KEYWORDS: biomass pyrolysis, fluidized bed, predictive model, pyrolysis process flowsheet simulation, reactor model.

INTRODUCTION

Conversion of raw biomass into useful chemicals requires certain conditions to optimize the yield of desired products.[1] Pyrolysis, the heating of biomass in the absence of oxygen, produces solid (char), liquid (tar), and gaseous products in various ratios depending on the temperature and residence time, as well as the chemical makeup of the feed. At relatively high temperatures and short residence times, the yield of liquid bio-oil is maximized, and this is currently the most desired product for its fuel value and the chemical precursors it contains.[2]

Fluidized beds are well suited to the fast pyrolysis of biomass. Their high heat and mass transfer rates enable precise temperature control and ensure uniform reaction of biomass particles, while pyrolysate vapor can be quickly removed and quenched to maximize the yield of desired product and minimize the extent of secondary gas-phase reactions.[1] Because of the multiscale nature of the reacting system, modeling biomass pyrolysis in a fluidized bed is no trivial task. The heat transfer, mass transfer, and reactions occurring within a biomass particle must be balanced with the macroscopic hydrodynamics and heat transfer within and without the fluidized bed.

A wide range of approaches for modeling biomass pyrolysis in fluidized beds has been proposed in recent years.[3-4] These may be broadly divided into two groups: first principles and empirical.

First principles models almost all involve computational fluid dynamics (CFD), a single-particle model, or some combination of the two. CFD models can accurately replicate the hydrodynamics of the fluidized bed, although the hydrodynamics are typically only validated against non-reactive "cold beds."[3] These models use highly simplified reaction sets that only provide the basic distribution between solid, liquid and vapor products to keep the computational load from being excessive.[5-6] Most recent examples of such models[7-11] use similar reaction sets with only three reactants (cellulose, hemicellulose, and lignin) and three products (char, tar, and gas). Such models may predict heat transfer and biomass particle behavior within the bed with a high degree of accuracy but cannot be usefully integrated with process models of further downstream operations, such as product purification. Single-particle models depict the complex reactions and heat- and mass-transfer occurring within a physically realistic biomass particle with a high degree of accuracy,[12] but are difficult to scale-up across the number of different particles and varying conditions needed to depict industrial scale production.[13] While a combined CFD-single-particle model may provide the most accurate possible depiction of biomass pyrolysis in a fluidized bed reactor, the computation involved is time-consuming, making it impractical for integration into a larger process model. Pecha et al.[14] demonstrated the effectiveness of a coupled particle- and reactor-scale model, but limited their reaction set to only five reactions producing five non-specific products (primary and secondary char, bio-oil, and primary and secondary gas) in order to maintain a manageable computational load.

The most common way to integrate a pyrolysis reactor into a whole-plant model is to assume yields based on experimental results.[15] The drawback to using experimental yields is that, with the infinite variety of biomass compositions and reactor conditions, such a model is only applicable to the very specific biomass and reactor from which the data were derived.

A model that could straddle the gap between the first principles and empirical models cited above would use commercial process simulator tools and more detailed reaction kinetics to approximate the conditions of a fluidized bed without time-intensive calculations. Peters et al.[16] presented such a model, assuming that the fluidized bed behaves like an isothermal continuous stirred-tank reactor (CSTR). Their model, implemented in Aspen Plus, includes nine reactant and 24 product species based on a reaction network described by Di Blasi,[3] allowing it to be used for meaningful modeling of downstream processes. However, it treats biomass as a continuum without any particle size information and so is incapable of considering the effects of bed hydrodynamics such as elutriation.

To facilitate the development of commercial scale pyrolysis reactors, this work describes a novel approach to modeling noncatalytic solid pyrolysis reactions in a fluidized bed mostly made up of inert material. In this case, fluidized sand is maintained at a constant temperature while biomass particles circulate within it, decreasing in density as they pyrolyze until they are elutriated. Because the pyrolysis reactions considered are independent of the vapor phase, the exact location of a biomass particle within the bed is not important so long as the bed is well-mixed and maintained at a constant temperature. Consequently, it is possible to avoid coupling bed hydrodynamics with reaction kinetics and close the material and energy balances by lumping the biomass particles within the bed based on their residence time. Conditions for a given parcel of biomass particles following its introduction into the fluidized bed can be compared to multiple isothermal reactors in series, by means of which temperature is increased over uniform, small time steps. The temperature at each interval is estimated using an energy balance, while a kinetic scheme like that of Ranzi et al. (I)[17] of the CRECK Modeling Group at Politecnico di Milano is used to calculate the extents of pyrolysis reactions. The biomass density and particle size

distribution (PSD) are tracked in each reactor, and elutriation between stages is calculated using a method described by Kunii and Levenspiel.[18]

It bears repeating that the reactor model does not specifically address fluidized bed hydrodynamics, which does not have a direct impact on pyrolysis kinetics. Parameters related to bed hydrodynamics that are required by the reactor model may be taken from a "cold bed" fluidized bed model which, while not trivial, can be found as a standard unit operation block in commercially available process simulators. Furthermore, it assumes a spherical biomass particle shape for some calculations, which is an acknowledged limitation that may affect model predictions.

Implementation of this model should be straightforward in any commercially available process simulator. The fluidized bed may be modeled with a custom block combined with a built-in fluidized bed reactor or plug-flow reactor (PFR) block with a recycle stream, while the separations section may be modeled with appropriate built-in unit operation blocks.

MODEL DEVELOPMENT

The model proposed here does not attempt to simulate the hydrodynamics of the fluidized bed. Rather, it closes the heat and mass balances within the fluidized bed reactor by calculating the extents of the pyrolysis reactions as functions of biomass particle residence time. It is sufficient to include bed hydrodynamics so far as modeling a "cold bed" to ensure proper fluidization, for which there are multiple existing models that are widely available. The fundamental assumption is that the solid pyrolysis reactions are independent of those in the gas phase. The biomass can thus be treated as existing within an isothermal medium of fluidizing gas and sand. In addition,

it is further assumed that the biomass particles are spherical and small enough that heat transfer is the same in all directions.

Because pyrolysis reactions are highly temperature-dependent, the biomass within the bed is tracked in a series of small time steps as it is heated from the feed temperature to the temperature of the bed. **Figure 1** illustrates how the model treats these time steps. Each time step of length τ (s) includes a heat and mass balance around the solid biomass particles. Although the particles are dispersed throughout the bed, they all are subjected to the same surroundings: the sand and fluidizing gas are maintained at a constant temperature. Because of this, the biomass particles may be categorized with respect to their residence time to significantly decrease the computational intensity of the model. Within each time step, the reaction rate is determined by the biomass temperature and biomass contents at that time step. Consequently, the process of heating and decomposing the biomass can be simulated as a large number of PFRs in series, each having a residence time τ, with elutriation calculations performed after each reactor to determine the amount of biomass that remains to move on to the next one. Once the biomass reaches the temperature of the bed, its attrition, elutriation, and further pyrolysis can be modeled at the bed temperature. The freeboard contains only vapor and elutriated particles that flow in the same direction with approximately the same velocity, and so is treated as an adiabatic PFR.

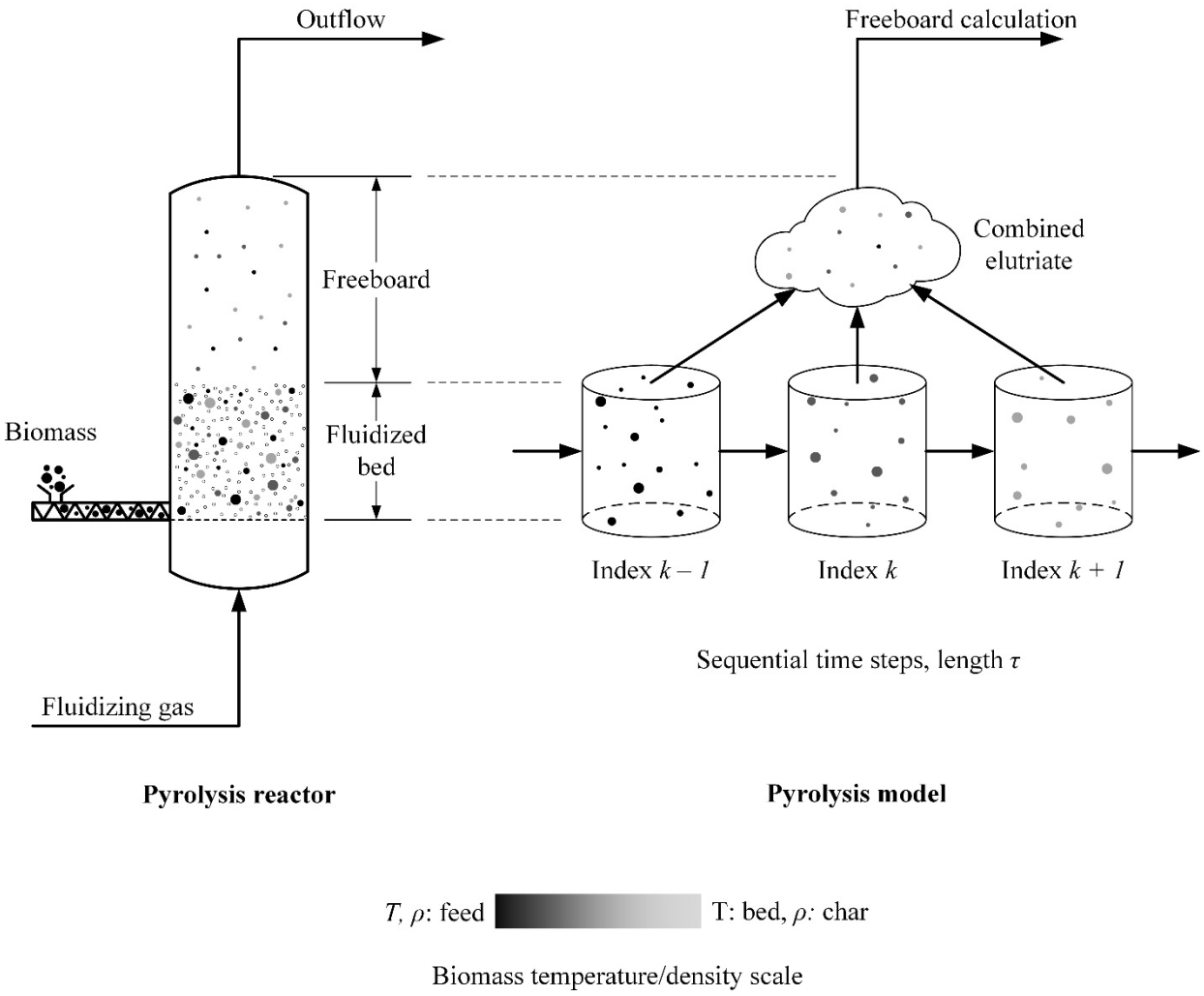

Figure 1 Diagram of the fluidized bed reactor as modeled. The leftmost block represents the entire reactor with sand (hollow circles) included. To the right are three consecutive time steps showing biomass particles only (solid circles) for clarity. Elutriated particles are collected in a combined stream represented by the single box above the three time steps. With time, the biomass temperature approaches that of the bed and its density decreases. Both phenomena (increasing temperature, decreasing density) are illustrated by the change in shading, although they are not directly proportional.

Energy balance around biomass

The rate at which heat is transferred into the biomass particles by convection as they pass through the k^{th} time step, $\dot{q}_{t,k}$ (kJ/s), is balanced by the rate at which it is consumed by the endothermic pyrolysis reactions, $\dot{q}_{r,k}$ (kJ/s), plus the rate at which it is absorbed, $\dot{q}_{a,k}$ (kJ/s), which changes the temperature of the biomass itself:

$$\dot{q}_{t,k} = \dot{q}_{r,k} + \dot{q}_{a,k} \tag{1}$$

Using sufficiently small time increments, the rate of heat absorption by the biomass as it passes through the k^{th} time step can be approximated by

$$\dot{q}_{a,k} = \dot{M}_k C_{P,k}(T_{k+1} - T_k) \tag{2}$$

Where $\dot{M}_k$ (kg/s) is the mass flow rate of biomass entering the k^{th} step, $C_{P,k}$ (kJ/kg-K) the heat capacity of the biomass entering the k^{th} step, and T_{k+1} (K) the temperature of the biomass leaving and T_k (K) the temperature of the biomass entering the k^{th} time step. The rate at which heat is consumed by the endothermic pyrolysis reactions as the biomass passes through the k^{th} time step can be approximated by

$$\dot{q}_{r,k} = \sum_i \Delta h_{i,k}^f \Delta \dot{m}_{i,k}^r \tag{3}$$

where $\Delta h_{i,k}^f$ (kJ/kg) is the heat of formation of the i^{th} component at the temperature and pressure of time step k, $\Delta \dot{m}_{i,k}^r$ (kg/s) is the change in mass flow rate due to reaction of the i^{th} component in time step k, and the product is summed for all i components. The change in mass flow rate is calculated with the equation:

$$\frac{\Delta \dot{m}_{i,k}^{r}}{W_i} = \sum_{n} \nu_{i,n} \frac{r_{n,k}}{W_n} \tag{4}$$

where W_i and W_n are the molecular weights of component i and the reactant of reaction n, respectively, $\nu_{i,n}$ is the stoichiometric coefficient of component i in reaction n (negative if component i is consumed or positive if it is generated), and $r_{n,k}$ (kg/s) is the rate of the n^{th} reaction at the temperature of the k^{th} step. The reaction rates are calculated using the equation:

$$r_{n,k} = A_n T_k^{x_n} e^{-\left(\frac{E_n}{R_C T_k}\right)} \dot{m}_{n,k} \tau \tag{5}$$

where A_n (K^{-x_n}/s) is the pre-exponential coefficient and x_n is the pre-exponential temperature exponent for the rate of the n^{th} reaction, E_n (kcal/kmol) is the activation energy of the n^{th} reaction, R_C is the universal gas constant (kcal/kmol-K), $\dot{m}_{n,k}$ (kg/s) is the mass flow rate of the biomass reactant consumed in the n^{th} reaction that is entering the k^{th} step, and τ (s) is the length of the k^{th} step. The reactions and their corresponding pre-exponential parameters and activation energies were adapted from Ranzi et al. (I)[17] and tabulated by Caudle et al.[19] (see Supporting Information).

It has been widely noted that ash has a catalytic effect on pyrolytic decomposition reactions, and Ranzi et al. (I)[17] introduced a term to adjust the activation energy of certain reactions to account for this effect. First, a biomass-specific ash factor, F_a (dimensionless) is defined as:

$$F_a = \tanh\left(\frac{pct_{ash}}{2}\right) \tag{6}$$

where pct_{ash} is the mass percent of ash in the biomass. The ash factor is used to adjust the activation energy of reactions 2, 4, and 8 in Ranzi et al. (I)'s kinetic scheme[17] via the equation:

$$E_n = E_n^0 - \mathrm{B}(F_a - 0.5) \tag{7}$$

where E_n^0 (kcal/kmol) is the original value for the activation energy of the reaction and B (kcal/kmol) is an empirical constant with a value of 600 for reaction 2 and 1000 for reactions 4 and 8.[17] For any species with an appreciable amount of ash, the inclusion of ash catalysis has the effect of increasing the production of light species at the expense of larger, more valuable products.

The rate at which heat is transferred from the fluidized bed to the biomass as it passes through the k^{th} time step (see equation (1)) is also equal to

$$\dot{q}_{t,k} = h_{p,k} a_k (T_B - T_k) \tag{8}$$

where $h_{p,k}$ (kJ/m^2-s-K) is the convective heat transfer coefficient and a_k (m^2) the heat transfer area as the biomass passes through the k^{th} time step, and T_B (K) is the fluidized bed temperature. To simplify the calculation of a_k, which is not a sensitive parameter for the overall performance of the model, it is assumed that biomass is fed as roughly spherical particles of uniform diameter (in reality, the biomass has a PSD). Thus, a_k can be estimated from the mass flow rate of biomass entering the k^{th} step, $\dot{M}_k$, the density of the biomass entering the k^{th} time step, $\rho_{b,k}$ (kg/m^3), and the mass-weighted mean diameter of the biomass particles entering the k^{th} time step (calculated from the PSD at the k^{th} time step), $d_{p,k}$ (m), with the equation:

$$a_k = \frac{6\dot{M}_k \tau}{\rho_{b,k} d_{p.k}} \tag{9}$$

A full derivation of equation (9) is included in the Supporting Information.

Substituting the appropriate terms into equation (1) and rearranging, a solution for T_{k+1} yields:

$$T_{k+1} = T_k + \frac{\left(\frac{6\dot{M}_k \tau h_{p,k}}{\rho_{b,k} d_{p,k}}(T_B - T_k) - \sum_i \Delta h_{i,k}^f \Delta \dot{m}_{i,k}^r\right)}{\dot{M}_k C_{P,k}} \tag{10}$$

The exit point for this initial heating process is when the biomass reaches a temperature within 0.1% of the difference between its feed temperature and the temperature of the sand bed. At this point, the biomass is almost completely pyrolyzed and any further reactions are assumed to occur under isothermal conditions

In this model Kunii and Levenspiel's correlation for the Nusselt number of a spherical particle suspended in a gas flow is used to estimate the convective heat transfer coefficient, $h_{p,k}$:[18]

$$\mathrm{Nu}_k = \frac{h_{p,k} d_{p,k}}{k_g} = 2 + F\,\mathrm{Re}_{p,k}^{1/2}\mathrm{Pr}^{1/3} \tag{11}$$

Here Nu_k is the Nusselt number for the k^{th} time step, k_g (kJ/m-s-K) is the thermal conductivity of the fluidizing gas, F is a factor between 0.6 (that for a single suspended particle) and 1.8 (that for a fixed bed), $\mathrm{Re}_{p,k}$ is the Reynolds number for a particle with diameter $d_{p,k}$ suspended in the fluidizing gas, and Pr is the Prandtl number of the fluidizing gas. The particle Reynolds number as defined by Kunii and Levenspiel for this correlation is[18]

$$\mathrm{Re}_{p,k} = \frac{d_{p,k} u_0}{\nu_g} \tag{12}$$

where u_0 (m/s) is the superficial velocity of the fluidizing gas and ν_g (m^2/s) its kinematic viscosity. The Prandtl number of the fluidizing gas is defined as

$$\mathrm{Pr} = \frac{C_{P,g}\mu_g}{k_g} \tag{13}$$

where $C_{P,g}$ (kJ/kg-K) is the fluidizing gas heat capacity and μ_g (Pa-s) its viscosity. Setting the value of F in equation (11) to 0.8 and solving for the convective heat transfer coefficient:

$$h_{p,k} = \frac{k_g}{d_{p,k}}\left(2 + 0.8\,\mathrm{Re}_{p,k}^{1/2}\mathrm{Pr}^{1/3}\right) \tag{14}$$

Mass balance around biomass

Having established an energy balance, the next consideration is the material balance. The biomass is continually decomposing as it heats up, losing mass due to the evolution of volatile pyrolysis products. The change in total biomass flow rate due to reaction as it passes through the k^{th} time step, $\Delta\dot{M}_k^r$ (kg/s) can be calculated from the changes in mass flow rate due to reaction of the individual biomass components:

$$\Delta\dot{M}_k^r = \sum_{i \text{ in biomass}} \Delta\dot{m}_{i,k}^r \tag{15}$$

These include ash, which is inert with respect to pyrolysis, and char, which is assumed to partially replace some of the pyrolyzed biomass components as they decompose. Volatile pyrolysis products are assumed to be released immediately into the vapor phase, which is dealt with separately.

Experimental evidence suggests that biomass particles undergoing the first stages of pyrolysis in a fluidized bed lose mass while retaining their size.[20] Consequently, biomass particles that have just entered the reactor are assumed not to shrink in size as they are heated up to the bed

temperature and evolve volatile products, but to have shrinking density. Knowing the change in biomass flow rate as it passes through the k^{th} time step, the density of the biomass exiting that time step can then be calculated as follows:

$$\rho_{b,k+1} = \frac{\dot{M}_k + \Delta\dot{M}_k^r}{\dot{M}_k}\rho_{b,k} \tag{16}$$

Elutriation is a separate process from volatiles evolution, by which solid particles near the surface of the bed that have sufficiently low terminal velocities are entrained in the fluidizing gas and consequently removed from the fluidized bed. The effect of removing biomass particles before they are fully pyrolyzed should not be ignored, since a significant amount of elutriation will have an impact on the average residence time and, thus, the product distribution.

As alluded to earlier, biomass must be ground to size for fluidization and will, therefore, have a distribution of particle sizes, typically classified into particle diameter ranges. While the PSD is ignored in the first part to avoid drastically complicating the energy balance, it is an essential part of the elutriation mechanics. The effects of elutriation on the biomass particles during the k^{th} step are considered after the effects of volatilization have been determined and imposed. The mass rate of elutriation of biomass particles in each particle size class *j* elutriated during time step k, $\Delta\dot{m}_{j,k}^e$ (kg/s) is:

$$\Delta\dot{m}_{j,k}^e = \dot{m}_{j,k}^e \kappa_{j,k} \tau \tag{17}$$

where $\dot{m}_{j,k}^e$ (kg/s) is the mass flow rate of solids in size class *j* remaining after reaction in time step k, and $\kappa_{j,k}$ (s^{-1}) is a fractional elutriation rate constant. The elutriation rate constant is determined using the method outlined by Kunii and Levenspiel,[18] which begins by calculating a dimensionless particle diameter, $d_{j,k}^*$ for each size class *j* for each time step k:

$$d_{j,k}^{*} = d_j \left(\frac{\left(\rho_{b,k} - \rho_g\right) g}{\nu_g^2 \rho_g} \right)^{\frac{1}{3}} \tag{18}$$

where d_j (m) is the characteristic particle diameter of size class j (upper limit of size range for size class j arbitrarily chosen), ρ_g (kg/m^3) is the density of the fluidizing gas at the bed surface, and g (m/s^2) is the acceleration due to gravity. This dimensionless particle diameter is then used to calculate a dimensionless terminal velocity, $u_{j,k}^{*}$:

$$u_{j,k}^{*} = \left(\frac{18}{\left(d_{j,k}^{*}\right)^2} + \frac{2.335 - 1.744\ \Psi}{\sqrt{d_{j,k}^{*}}} \right)^{-1} \tag{19}$$

where Ψ is the sphericity of the biomass particles. The terminal velocity of the particle size class, $u_{j,k}^{t}$ (m/s) is calculated in turn using the equation:

$$u_{j,k}^{t} = u_{j,k}^{*} \left(\frac{\nu_g \left(\rho_{b,k} - \rho_g\right) g}{\rho_g} \right)^{\frac{1}{3}} \tag{20}$$

Finally, the general elutriation rate constant, $K_{j,k}$ (kg/m^2-s):

$$\mathrm{K}_{j,k} = \rho_g u_0 23.7 e^{-5.4 \frac{u_{j,k}^{t}}{u_0}} \tag{21}$$

is used to calculate the elutriation rate constant for each particle size class for the k^{th} time step:

$$\kappa_{j,k} = \begin{cases} 0 & u_{j,k}^{t} \geq u_0 \\ \dfrac{\mathrm{K}_{j,k}}{\rho_{b,k}(1 - \epsilon_B) L_B} & u_{j,k}^{t} < u_0 \end{cases} \tag{22}$$

where ϵ_B is the bed void fraction and L_B (m) the height of the fluidized bed.

Because the biomass is considered to have uniform composition across all particle sizes at each time step, the change in mass flow rate of a given component *i* due to elutriation, $\Delta\dot{m}_{i,k}^{e}$, is the sum of the fractional elutriation across all particle size classes multiplied by the mass remaining after reaction, or

$$\Delta\dot{m}_{i,k}^{e} = (\dot{m}_{i,k} + \Delta\dot{m}_{i,k}^{r}) \sum_{j} \kappa_{j,k}\tau f_{j,k} \tag{23}$$

where $f_{j,k}$ is the mass fraction of particles of size class *j* in time step *k*.

The mass flow rate of the i^{th} biomass component remaining in the bed after the k^{th} time step is thus described by the equation:

$$\dot{m}_{i,k+1} = \left(\dot{m}_{i,k} + \Delta\dot{m}_{i,k}^{r}\right) \sum_{j} \left(1 - \kappa_{j,k}\tau\right) f_{j,k} \tag{24}$$

The equations given above can be used to describe the mass and energy balance for biomass particles in a fluidized bed pyrolysis reactor and may be modified to apply to any fluidized bed in which solid decomposition reactions are independent of the vapor phase. However, the remaining solids will experience the same conditions as an isothermal PFR and can be simply modeled as such. They will also continue to be elutriated as they are further pyrolyzed, so it is important that the effects of elutriation be accounted for. To this end, the residence time of the PFR unit operation block tracking the biomass at constant temperature should be very small, and particles may then be elutriated from a solid recycle stream.

Implementation of the model in a commercial process simulator is illustrated in **Figure 2**. The fluidized bed reactor model consists of four blocks. Block TRamp is the "temperature-ramp"

section, which models the rapid heating of the biomass as it enters the bed. This is a customized unit operation block that must be built up from equations (1) through (24) following the conventions of the specific process simulator used. Block RX-01 is a customized PFR that accounts for the reactions that occur at constant temperature, and the associated solid-separation block, CY-01 calculates the elutriation of the remaining solids. Block CR-01 is a crusher block that simulates the attrition of biomass particles within the bed. Block RX-02 is the freeboard section of the reactor, also modeled as a PFR.

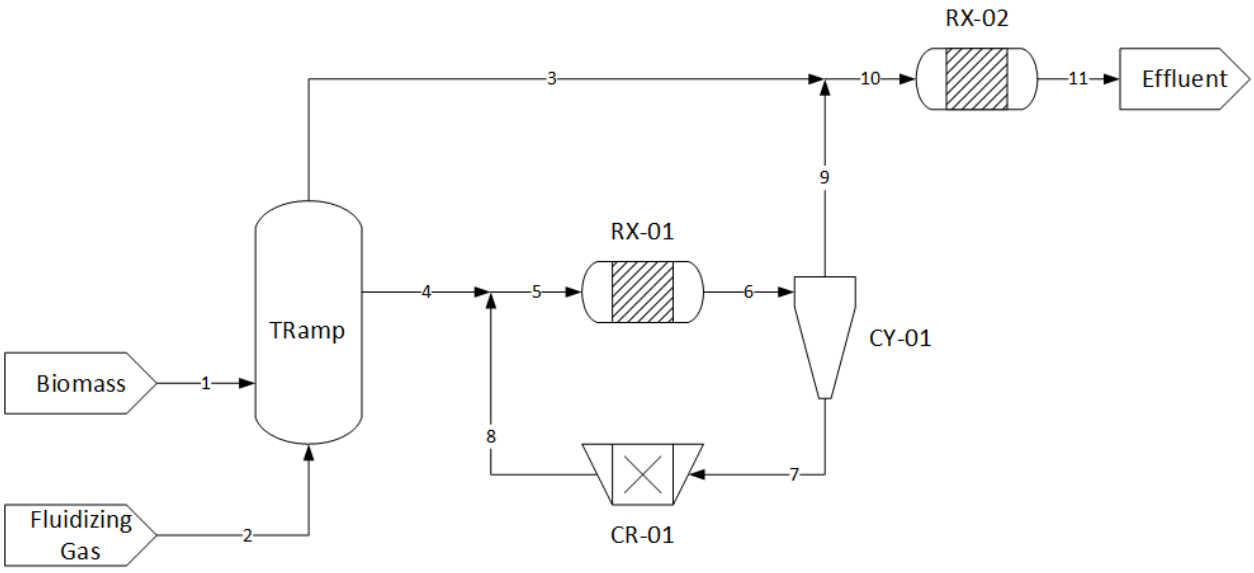

Figure 2 Fluidized bed biomass pyrolysis reactor model flow diagram.

Each block is set to the temperature of the fluidized bed, which is the apparent temperature of the sand and fluidizing gas and is assumed to be isothermal. Biomass enters at room temperature, while the pre-heated fluidizing gas enters at sufficiently higher pressure to overcome the pressure drop within the bed. An unspecified external heat source maintains the fluidized bed at the specified temperature with enough capacity to drive pyrolysis. Future work will address the use of partial oxidation of char and pyrolysis products as the heat source for autothermal operation.

All decomposition reactions adapted from Ranzi et al. (I)[17] are represented in the isothermal reactors, with the same rate expressions as seen in Equation (5). The residence time of RX-01 is set to 0.1 s to allow for a recycle loop that calculates elutriation. Since the only reactions that occur in RX-01 are slow pyrolysis reactions, on the order of many seconds to minutes, this residence time was arbitrarily chosen to allow for relatively rapid elutriation without overburdening the recycle loop. Future model iterations may look at the effect of residence time in the presence of more rapid reactions, e.g., partial oxidation. The elutriation rate (solid split fraction) in CY-01 is calculated in the same way as that in TRamp, using equations (17) through (23). Under the circumstances modeled, it is not important to match the observed rate of char elutriation, even if that data were available, as the char remaining in the bed is inert and behaves as a heat sink just like the sand. The parameters of the crusher are adjusted to approximate a slow rate of attrition, shifting the PSD to smaller diameters to maintain mass balance via char elutriation from the bed. The volume of the freeboard reactor block, RX-02 is taken directly from the geometry of the fluidized bed reactor.

RESULTS

Model Inputs

Model simulation results were compared to experimental data from the laboratory-scale reactor and separations systems described by Polin, Peterson et al.[21] Their setup can be succinctly characterized as a fluidized bed reactor followed by a cyclone and two condensers. Bed temperature was maintained at 500°C by means of clamshell electrical heaters. Biomass was fed into the reactor at 25°C and the fluidizing gas at 500°C and 40 in H_2O gauge (75 mm Hg gauge). The estimated dry, ash-free (DAF) compositions of the raw biomass used in the experiments in

terms of representative components (see Gorensek et al.[22] as well as the Supporting Information) are summarized in **Table 1**. These compositions were obtained by comparing the ultimate analyses of the biomass sources reported by Polin, Peterson et al.[21] and Polin, Carr et al.[23] with those of similar biomass sources compiled by Debiagi et al.[24] and averaging the representative compositions estimated by the latter.

Trace elements, i.e., "Other (N, S, ...)" were measured in the experimental biomass feed and pyrolysis products by ultimate analysis,[21, 23] but are not found in any of the model components of the kinetic mechanism,[17] nor are they included in the components used by Debiagi et al.[24] to construct representative compositions of biomass materials. As such, they were left out of the current model. Future efforts to account for these elements would require abandoning the current detailed kinetic model for a separate investigation of new kinetic pathways but would not affect the structure of the reactor model presented here.

Table 1 Ultimate analysis and composition of dry, ash free (DAF) biomass used in model simulations.

	Mass-% DAF biomass	
	Red Oak	Corn Stover
Ultimate Analysis		
Carbon	49.26	51.89
Hydrogen	4.99	5.35
Oxygen	45.57	41.44
Other (N, S, …)	0.18	1.31
Representative Composition		
TANN (tannin)	5.47	2.81
LIGC (C-rich lignin)	2.16	9.88
LIGH (H-rich lignin)	3.23	1.27
LIGO (O-rich lignin)	15.79	15.81
TGL (triglyceride)	3.92	7.62
XYHW (xylan hemicellulose)	27.07	25.48
CELL (cellulose)	42.36	37.14

The red oak biomass used by Polin, Peterson et al.[21] contained, in addition to the pyrolyzable biomass components, 0.87 mass-% ash (ASH) and was dried to 5.43 mass-% moisture (H2OL). It was fed into the reactor at a rate of 4.78 kg/hr. The corn stover used by Polin, Carr et al.[23] contained 9.65 mass-% ash and was dried to 2.43 mass-% moisture. It was fed into the reactor at a rate of 7.80 kg/hr. The red oak was crushed to a particle diameter range of 1 – 1680 μm with a

mass-weighted mean diameter of 430 μm, while no information is given for the corn stover, other than that it was less than 3.175 mm. To complete the model, the same PSD was used for both species, with the detailed distribution included in the Supporting Information. The fluidizing gas in both cases was pure nitrogen fed at a rate of 0.305 kmol/hr, approximately 115 standard L/min.

The laboratory-scale reactor used in both cases had an inner diameter of 8.9 cm and a total height of 83 cm. The reactor was filled with 1.6 kg of sand, with a particle size diameter range of 425–1180 μm and mass-weighted mean diameter of 745 μm. Simultaneous modeling of a nonreactive bed fluidized with the mixture of fluidizing gas and vapor products, using the Aspen Plus built-in FluidBed model, estimated a fluidized bed height of approximately 32 cm under these conditions, consistent with the experimental "reactor section" height of 31.1 cm.[21] The size of the freeboard section was thus estimated to be 8.9 cm in diameter by 51 cm in length. The volumetric flow rate within the freeboard changes based on the rate of volatiles evolution from the pyrolysis reactions, but a typical residence time of the freeboard is 0.5 s. Pressure drop within the bed was approximately 10 in H_2O, so blocks CR-01, CY-01, RX-01, and RX-02 (**Figure 2**) were maintained at 30 in H_2O gauge (56 mm Hg gauge). The crusher was modeled with a Rosin Rammler Sperling Bennet (RRSB) distribution function, with an RRSB dispersion parameter of 1.5 and a specific power of 5×10^{-6} J/kg. It should be noted that this power input is for matching the rate of attrition only, as the kinetic energy required to comminute the biomass particles is provided by collisions within the bed, which are in turn driven by the fluidizing gas.

The pyrolysis reactor was followed by a cyclone and two condensers to divide the products into solid, liquid, and vapor fractions. The cyclone was assumed to collect 99.9% of solids exiting the reactor, which are not returned to the bed. The laboratory-scale system had an electrostatic

precipitator following each condenser, but these were not explicitly modeled since the precipitators are needed to trap aerosols entrained in the vapor leaving the condensers~~, but~~ and the model unit operation blocks assume complete separation of the liquid and vapor phases.

Model Results

Polin, Peterson et al.[21] recorded several metrics for the operation of their laboratory-scale red oak pyrolysis reactor which were used to validate this model. These include the mass flow rates of the four product streams – biochar collected from the cyclone, heavy ends condensed at 125°C, light ends condensed at 12°C, and non-condensing gases (NCG) – the composition of the NCG stream as measured by micro gas chromatography (micro-GC), and the ultimate analysis of the biochar, light ends, and heavy ends. Polin, Carr et al.[23] recorded the same metrics for corn stover, but omitted the ultimate analysis of the biochar. Both sources reported the proximate analysis of their biomass feed and biochar, but the difference between volatile matter and fixed carbon cannot be converted into the model components used here.

As part of their analysis, Polin, Peterson, et al.[21] reported an enthalpy of pyrolysis for red oak of 1.59 kW, or 1.14 MJ/kg. The value of 2.02 kW, or 1.52 MJ/kg, calculated from the model is similar. Both the experimental and model results fall into the range of measurements for woody biomass reported by other sources, 0.7-1.75 MJ/kg.[25-26] The higher value from the model is an indication that the decomposition predicted by the kinetic scheme is more extensive than that observed experimentally. At these energy requirements, the experimental reactor does not suffer from limitations due to heat transfer into to the bed itself. When used for scale-up calculations, it is necessary to compare the enthalpy of pyrolysis calculated by the model to the ability to maintain the reactor at the desired temperature, which depends on the specific choice of heat

transfer equipment and media (external or internal heaters, gaseous or solid heat transfer media, etc).

Figure 3 illustrates the condition of the biomass within the reactor model for red oak pyrolysis. In **Figure 3a**, the temperature and density (left-hand axis) are plotted as functions of the time elapsed since a given batch of biomass particles entered the reactor. The mass quantity of biomass remaining in the fluidized bed (not yet volatilized or elutriated) is plotted using the right-hand axis. The temperature increases rapidly, with the first inflection indicating the point where the endothermic pyrolysis reactions take place. The fact that the density of the biomass decreases rapidly along with the total mass indicates that the majority of mass loss is due to the release of volatile products within the first 5 s. With τ set to 0.01 s, the biomass temperature reaches the temperature of the reactor after 531 steps (5.31 s), leaving char and a minimal amount of slow-reacting species such as TANN and LIGOH. The density is held constant from this point on, as subsequent attrition is more significant than any slight change in density due to further reaction, and as the char particles break down, they are gradually elutriated from the bed. The residence time of the fluidizing gas is relatively short, around 0.8 s. **Figure 3b** demonstrates the model's ability to track PSD. The biomass within the bed has a larger mean diameter than the feed, since small particles are preferentially elutriated. As residence time increases within the recycle loop, the mean diameter decreases due to the effects of attrition as modeled by the crusher.

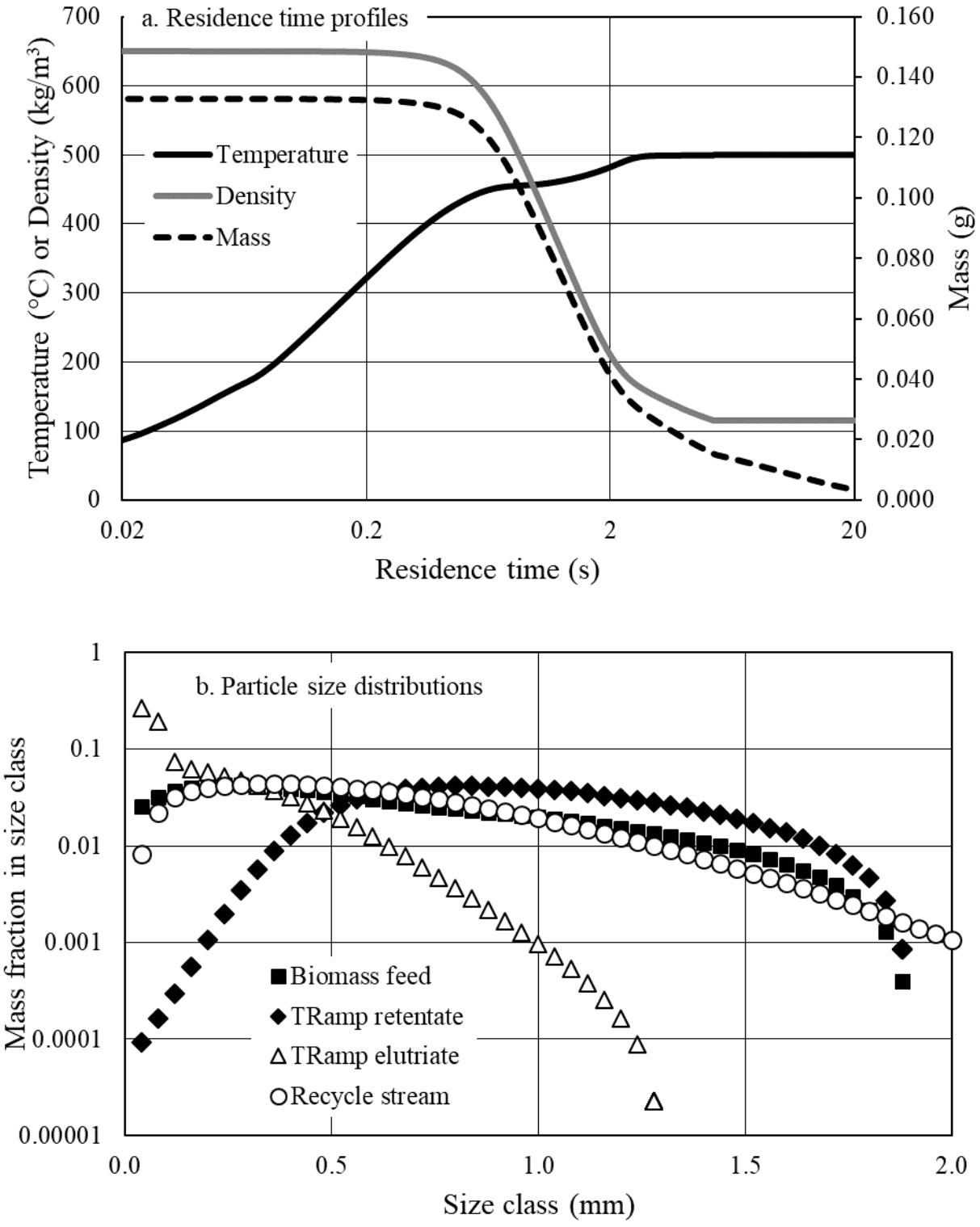

Figure 3 (a) Biomass temperature (black line), density (gray line), and mass quantity remaining (black dashed) as functions of residence time. The mass quantity at any given residence time

corresponds to the amount of biomass in the fluidized bed that has achieved that residence time. (b) Biomass PSD in the biomass feed (squares), elutriated from the TRamp block (triangles), remaining in the bed after reaching 500°C (diamonds), and within the constant temperature recycle loop (circles).

The distribution of the reactor outflow among the four product streams is displayed in **Figure 4**, comparing the model predictions and experimental results for both the red oak and corn stover. The values are reported as weight-percent product yields calculated on a moist biomass basis, i.e., both H2OL and ASH are included in the calculation of the initial and final mass. The fractions of pyrolysate recovered as biochar and heavy ends are very similar to those reported by Polin, Peterson et. al.[21] for red oak, while the fraction recovered as biochar is consistent with Polin, Carr et al.[23] for corn stover. The amount of light and heavy ends combined, the "whole bio-oil" fraction, is similar for both red oak and corn stover.

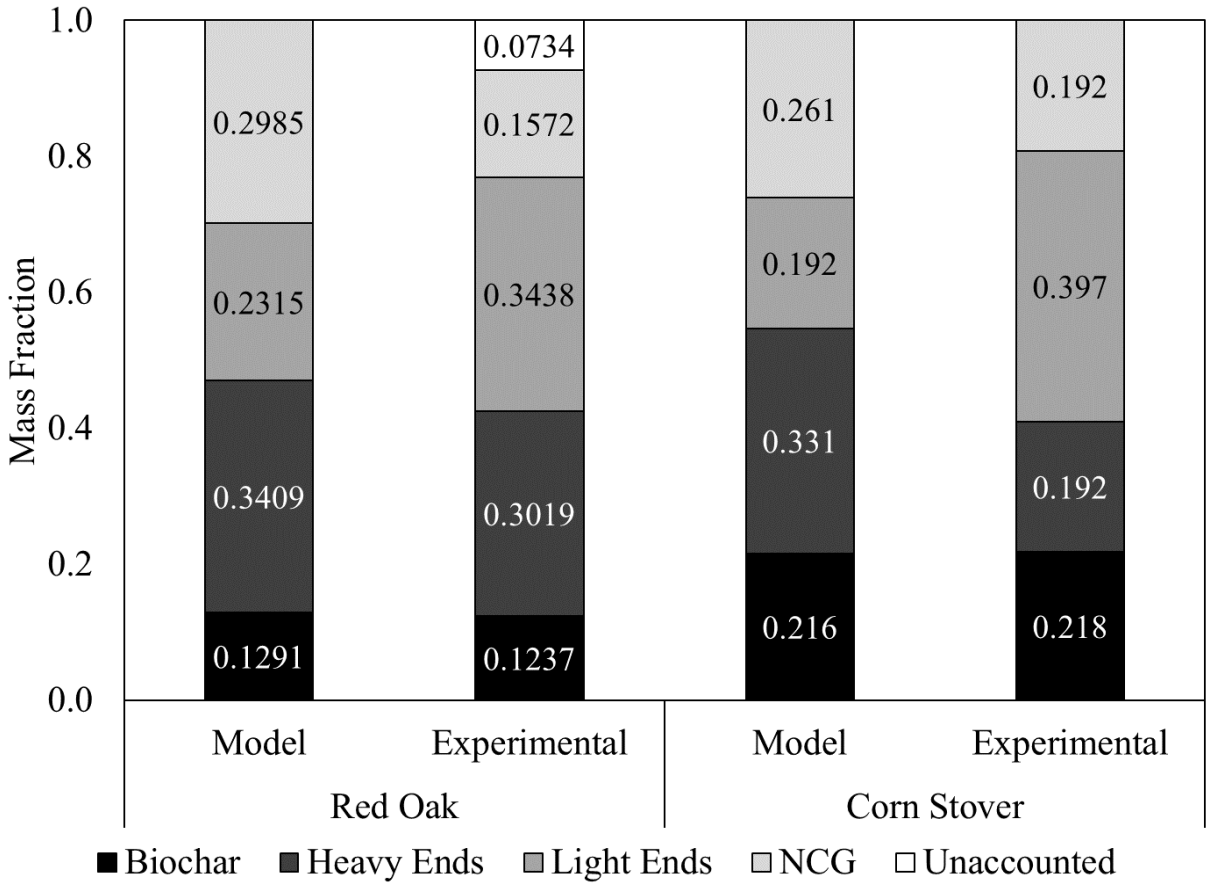

Figure 4 Distribution of pyrolysate products – comparison between model predictions and experimental results for red oak and corn stover.

The amount of light ends and NCG produced from red oak biomass as predicted by the model is correct in total but not in their respective quantities. This discrepancy is likely a result of the reaction set used. **Figure 5** compares the composition of the NCG fraction measured by Polin, Peterson et al.[21] and Polin, Carr et al.[23] to that predicted by the model. Although the fractional yields of CO, CO2, and CH4 are comparable for both red oak and corn stover, the model consistently contains much more "Other" – light hydrocarbons such as propionaldehyde (ALD3), ethylene (C2H4), and formaldehyde (CH2O). While it would be convenient to assume that these other species could be found in the "unaccounted" portion of the experimental mass balance,

there is no concrete evidence to back this up, nor does it completely account for the imbalance between the light ends and NCG, while the experiments with corn stover have zero unaccounted mass and experience the same issue. This suggests that the kinetic scheme of Ranzi et al. (I)[17] tends to overpredict the production of NCG by breaking the biomass into molecules that are smaller than those observed in these experiments.

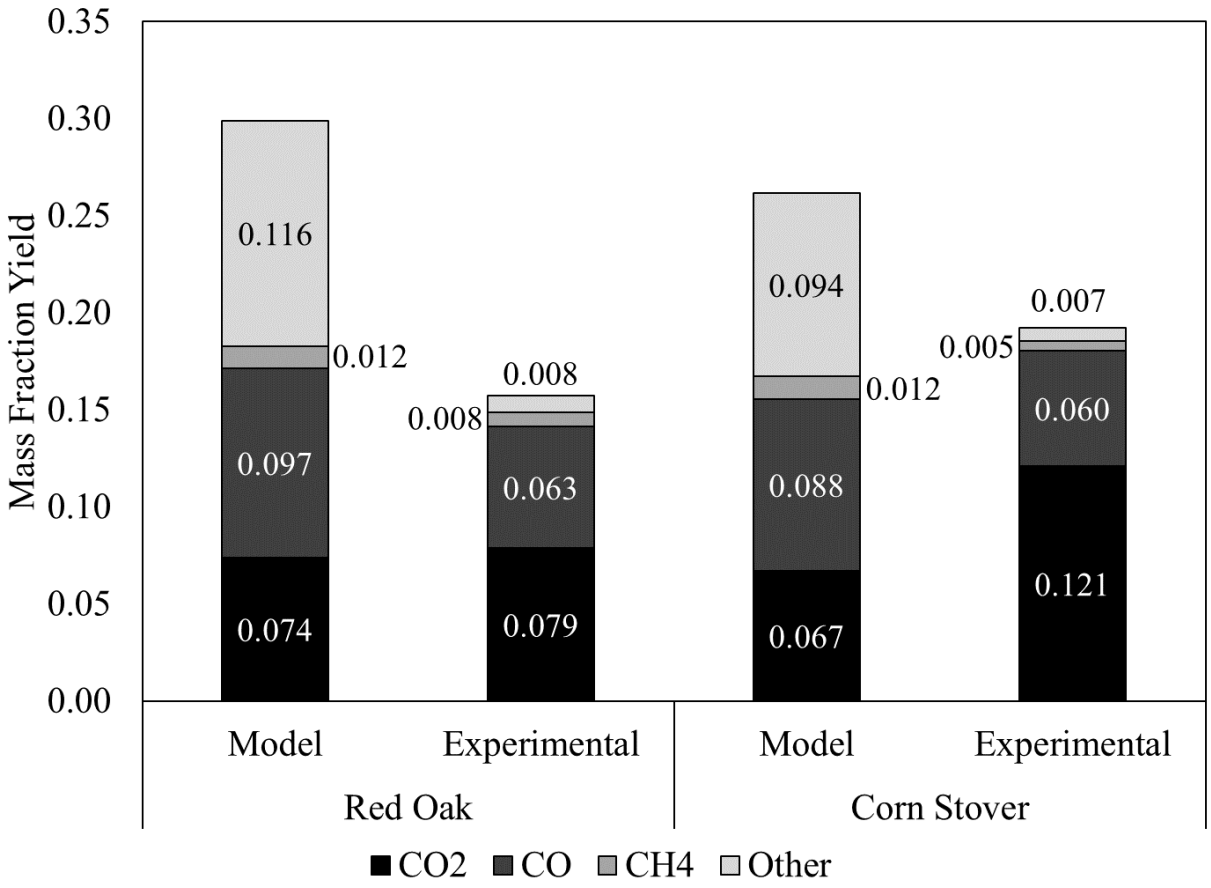

Figure 5 NCG composition – comparison between model predictions and experimental results for red oak and corn stover.

A full breakdown of the product distribution predicted by the fluidized bed reactor model for red oak pyrolysis is shown in **Figure 6**. The fractional yield of each species is represented by the

height of the associated bar, while the distribution of the species among the four product streams is indicated by its shading. Although the experimental data is not detailed enough to validate this information, it is a useful visualization of the extent to which the model can be leveraged to simulate even more detailed downstream separations.

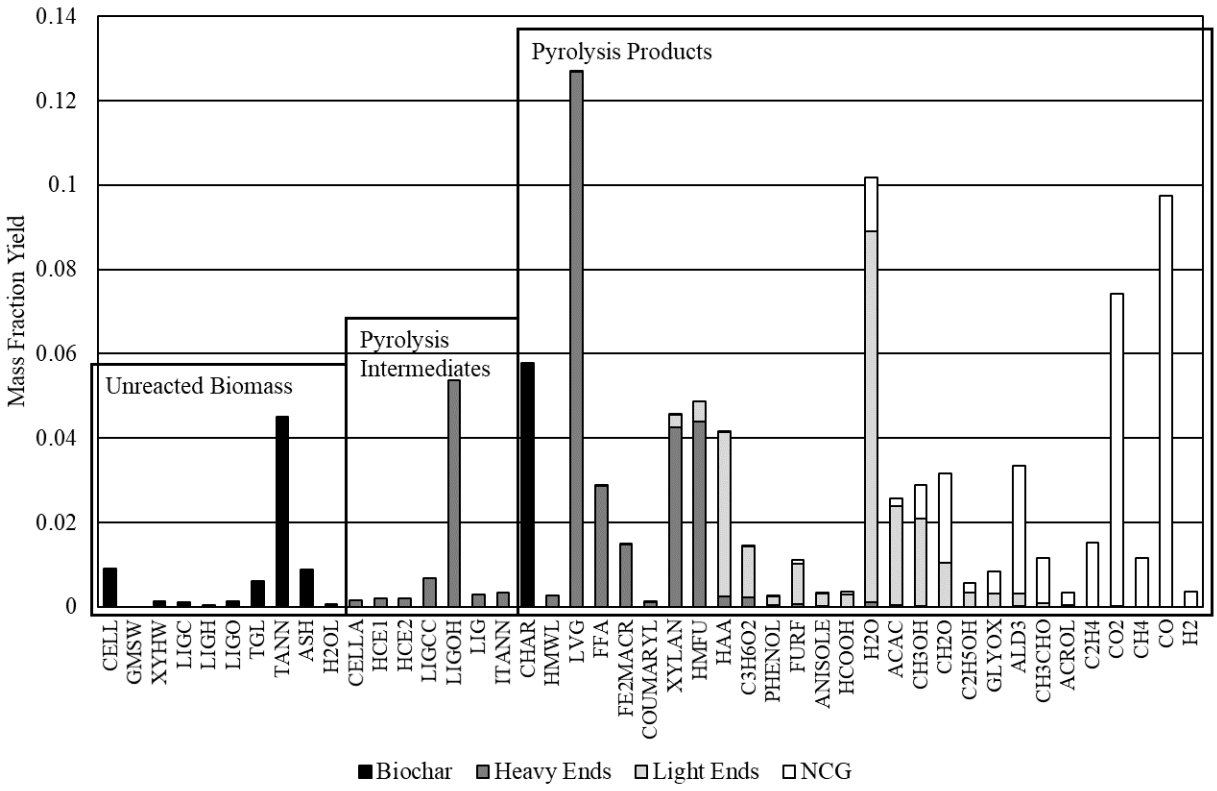

Figure 6 Product distribution predicted by the fluidized bed reactor model. Acronyms used are the same as those of Gorensek et al.[22]

Figure 7 compares the model results to experimental elemental compositions (which, unlike the ultimate analyses in **Table 1** include ash explicitly and separately) for the raw biomass, biochar, heavy ends, light ends, and combined liquid fractions produced by red oak pyrolysis. Note that the six fraction values above the plot area border represent small mass fractions at the very top of the stacked bars, the two left-most representing ash and the remaining four "Other." This

"Other" includes unaccounted mass, as in the discussion of **Figure 4**, and so is not necessarily limited to the trace elements counted in **Table 1**. Considering the small difference in original biomass composition – due to the restrictions of choosing representative structural components of the biomass rather than using a simple elemental makeup – the model results are very close to the experimental observations. Of particular interest is the similarity in composition of the whole bio-oil fractions. If a future reactor design has only one liquid product, leaving more precise fractional separation to later units, the similarity of the model and experimental results for this stream is particularly important.

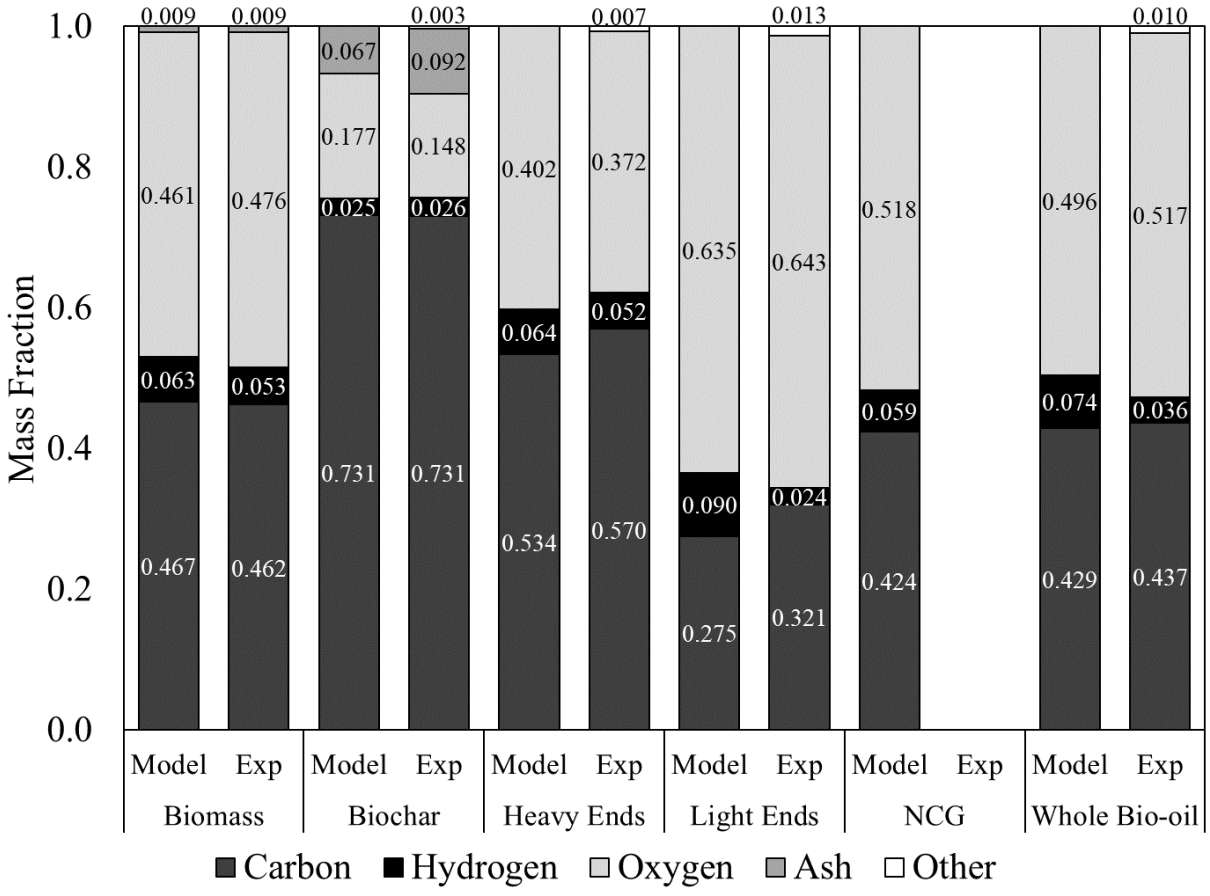

Figure 7 Comparison between predicted (Model) and experimental (Exp) C, H, and O compositions of process streams for red oak pyrolysis.

Figure 8 compares the model predictions and experimental results of the elemental composition for corn stover. Here, the three fraction values above the plot area border represent small mass fractions of "Other" at the very top of the stacked bars. While not as accurate as the results for red oak, the model maintains the relative distribution of oxygenated species between the heavy and light ends. Unfortunately, the elemental composition for the biochar was not reported.

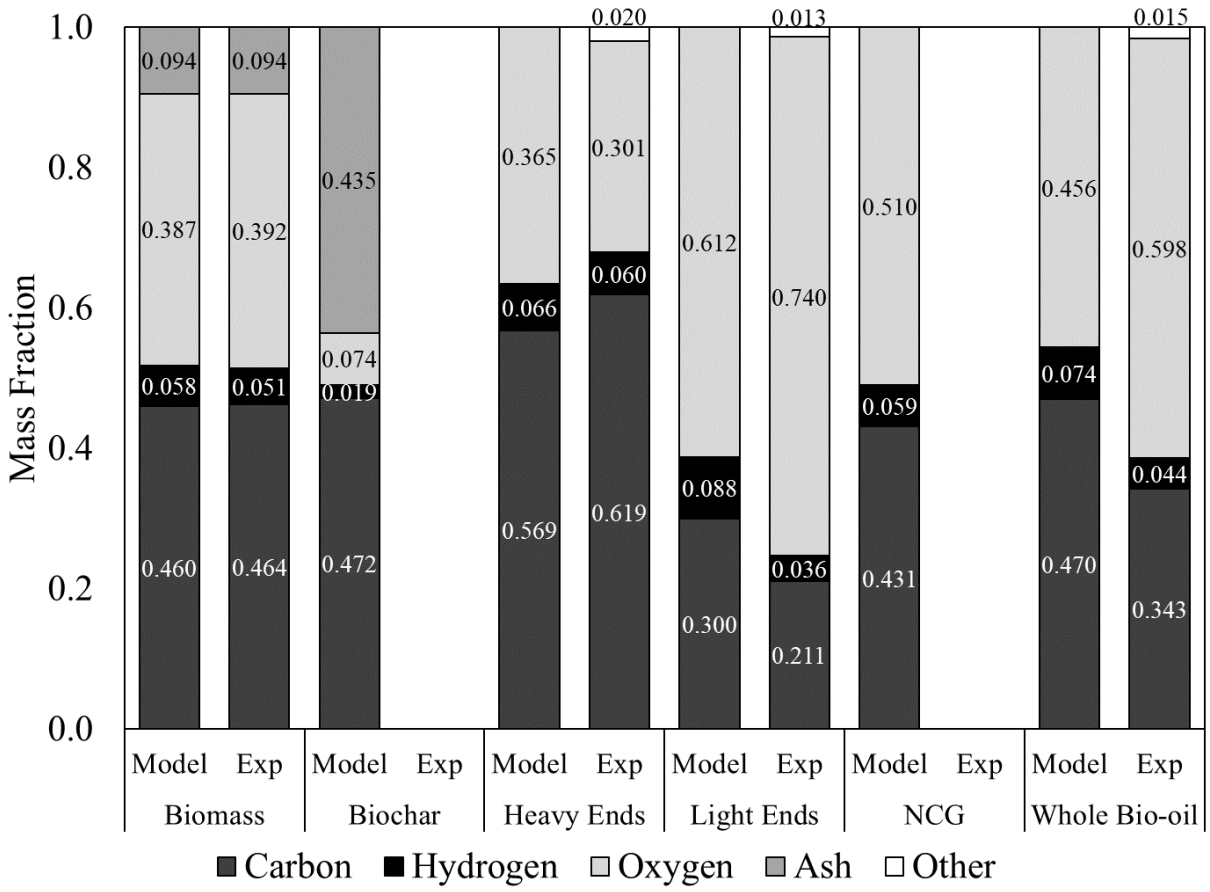

Figure 8 Comparison between predicted (Model) and experimental (Exp) C, H, and O compositions of process streams for corn stover pyrolysis.

The ability to simulate a variety of process conditions outside the range of experimental data, aiding in the design and optimization of new systems, is the most important factor in assessing the usefulness of a plant model. **Figure 9** demonstrates the sensitivity of product distribution to

the fluidized bed operating temperature. Bio-oil and NCG production increase rapidly with temperature initially, as higher temperature and resulting shorter residence times favor liquid and vapor products over char formation. As the temperature increases beyond the generally accepted approximate optimum of 500°C, the amount of bio-oil produced peaks and begins to decline while the amount of NCG produced continues to increase. These trends result in an optimum selectivity for bio-oil production at approximately 480°C for red oak and 520°C for corn stover.

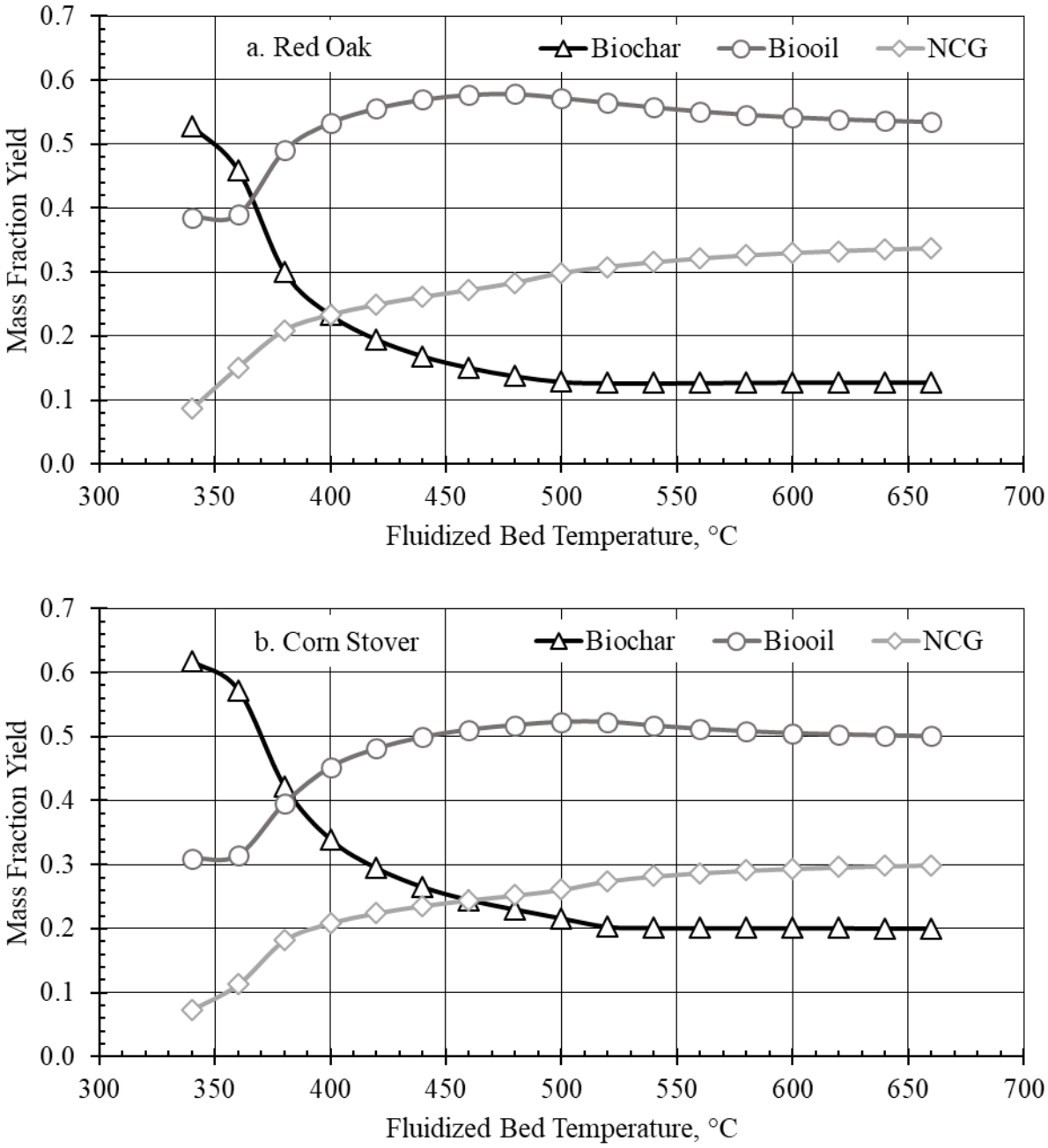

Figure 9 Model-predicted pyrolysis product distribution as a function of fluidized bed operating temperature for two different biomass sources: a. Red Oak; b. Corn Stover.

DISCUSSION

While there are discrepancies between the model and experimental results regarding the distribution of light ends and NCG, the estimation of the yield of the highest value-added products in the heavy ends is very close. The Ranzi kinetic model is the most accurate model of biomass thermal decomposition readily applicable in commercial process simulators, and modification of this model or creation of a new one to match this experimental data might improve the agreement but is beyond the scope of this work.

The current use of a mean particle diameter for calculation of biomass heating rates was implemented to avoid the need to track the temperature and perform unique reaction rate calculations for dozens of particle size classes over hundreds or thousands of time intervals. This introduces a small but unknown amount of error, mitigated by the fact that the PSD is continually narrowing as the smallest particles are quickly elutriated from the bed. In the future it may be viable to invest the time needed to implement this tracking capability to test the validity of its exclusion.

Ranzi et al. (II) developed a model for secondary gas-phase reactions,[27] but these kinetics were not implemented in the current model for two reasons. First, they are relatively slow compared to the less than one-second residence time of vapor in the fluidized bed reactor, an observation made by the developers of the experimental reactor. The second is that they tend to increase the amount of NCG by further decomposing components of the condensable products, which would decrease the agreement of the current model with experimental results.

In their original kinetic scheme, Ranzi et al. (I)[17] included several intermediate species that are initially trapped within a metaplastic phase. These species are released to the vapor phase as conventional components, but in the metaplastic state they do not have defined thermophysical

properties. Because their lack of thermophysical properties makes them impossible to implement while maintaining a grounded energy balance and the high temperatures of the pyrolysis reactor in question makes the release of metaplastic species nearly instantaneous, these reactions have been ignored by many works using this kinetic scheme.[19, 28] Many of the released species are found in the NCG stream, so preventing the metaplastic intermediates from being released as such would be beneficial to the model agreement with experimental results. This would require significant alteration to the kinetic scheme, however, and so is beyond the scope of this reactor modeling effort.

It is sufficient at this point that the fluidized bed reactor model is able to predict the energy usage of pyrolysis and the product distribution with enough detail to facilitate the design of more complex downstream separation processes. Reducing the thousands of components that make up raw biomass into eight representative components necessarily introduces an amount of error into the elemental makeup of the products. In exchange, the components are given physical structure and thermodynamic properties that allow for the calculation of rigorous mass and heat balances. The specific products evolved are thus well defined and may be processed in any manner of unit operations.

This model also leaves open the possibility of converting the simulated reactor from externally heated to autothermal operation. Polin, Peterson, et al.[21] successfully demonstrated the ability to overcome heat transfer limitations into the bed by operating the reactor under autothermal conditions. Admitting a small amount of oxygen into the reactor allowed the enthalpy of combustion to be supplied by the exothermal oxidation of char and some of the lighter pyrolysis products. In this reactor model, it would be assumed that the evolution of pyrolysis products would preclude oxygen from reaching the biomass before the majority of decomposition

reactions could reach completion. In that case, the inclusion of appropriate reactions in blocks RX-01 and RX-02 could account for oxidation within the fluidized bed and freeboard respectively. There is currently no kinetic scheme for the oxidation of the more complex components involved in this model that could be directly implemented in a process simulator. Development of such a scheme would be the next step before this model could simulate such processes.

CONCLUSIONS

The model presented here balances the two major criteria for design and optimization of a biomass pyrolysis plant in commercial process simulators. It accurately predicts the energy requirements of pyrolysis and includes a wide range of products, allowing for detailed modelling of downstream bio-oil processing. Despite the level of detail, it is simple enough to be implemented in commercial process simulation software, allowing easy design and optimization of a variety of reactor conditions, possible feedstocks, and plant layouts. The decomposition reaction model can be easily modified, if desired, to include future advances. Most importantly, the reactor model allows for the future implementation of oxidation reactions to simulate autothermal pyrolysis.

ASSOCIATED CONTENT

Supporting Information.

Derivation of equation (9), lists of chemical species, pyrolysis reactions and kinetics used in

reactor model, biomass feed particle size distribution plot, and complete nomenclature key.

MS sc-2020-057834 Supporting Info.pdf

AUTHOR INFORMATION

Corresponding Author

* Maximilian B. Gorensek. Phone: +1 803 725-1314; Email: maximilian.gorensek@srnl.doe.gov.

ORCID

Benjamin Caudle: 0000-0003-1502-717X

Maximilian B. Gorensek: 0000-0002-4322-9062

Chau-Chyun Chen: 0000-0003-0026-9176

Author Contributions

The manuscript was written through contributions of all authors. All authors have given approval to the final version of the manuscript. All authors contributed equally.

Funding Sources

Funding support was provided by the US Department of Energy under grant DE-EE0007888-02-7. C.-C.C. and B.C. gratefully acknowledge the financial support of the Jack Maddox Distinguished Engineering Chair Professorship in Sustainable Energy, sponsored by the J.F Maddox Foundation. SRNL is operated for the DOE's Office of Environmental Management (DOE-EM) by Savannah River Nuclear Solutions, LLC, under Contract DE-A C09-08SR22470.

Notes

The authors declare no competing financial interest.

ACKNOWLEDGMENT

This report was prepared as an account of work sponsored by an agency of the United States Government. Neither the United States Government nor any agency thereof, nor any of their employees, makes any warranty, express or implied, or assumes any legal liability or responsibility for the accuracy, completeness, or usefulness of any information, apparatus, product, or process disclosed, or represents that its use would not infringe privately owned rights. Reference herein to any specific commercial product, process, or service by trade name, trademark, manufacturer, or otherwise does not necessarily constitute or imply its endorsement, recommendation, or favoring by the United States Government or any agency thereof. The views and opinions of authors expressed herein do not necessarily state or reflect those of the United States Government or any agency thereof. The United States Government retains and the publisher, by accepting this article for publication, acknowledges that the United States Government retains a non-exclusive, paid-up, irrevocable, worldwide license to publish or reproduce the published form of this work, or allow others to do so, for United States Government purposes.

REFERENCES

1. Bridgwater, A. V., Review of fast pyrolysis of biomass and product upgrading. *Biomass and Bioenergy* **2012,** *38*, 68-94 (https://doi.org/10.1016/j.biombioe.2011.01.048).
2. Venderbosch, R.; Prins, W., Fast pyrolysis technology development. *Biofuels, Bioproducts and Biorefining* **2010,** *4* (2), 178-208 (https://doi.org/10.1002/bbb.205).
3. Di Blasi, C., Modeling chemical and physical processes of wood and biomass pyrolysis. *Progress in Energy and Combustion Science* **2008,** *34* (1), 47-90 (https://doi.org/10.1016/j.pecs.2006.12.001).
4. Gómez-Barea, A.; Leckner, B., Modeling of biomass gasification in fluidized bed. *Progress in Energy and Combustion Science* **2010,** *36* (4), 444-509 (https://doi.org/10.1016/j.pecs.2009.12.002).

5. Sharma, A.; Wang, S.; Pareek, V.; Yang, H.; Zhang, D., Multi-fluid reactive modeling of fluidized bed pyrolysis process. *Chemical Engineering Science* **2015,** *123*, 311-321 (https://doi.org/10.1016/j.ces.2014.11.019).
6. Zhong, H.; Xiong, Q.; Yin, L.; Zhang, J.; Zhu, Y.; Liang, S.; Niu, B.; Zhang, X., CFD-based reduced-order modeling of fluidized-bed biomass fast pyrolysis using artificial neural network. *Renewable Energy* **2020,** *152*, 613-626 (https://doi.org/10.1016/j.renene.2020.01.057).
7. Xue, Q.; Heindel, T. J.; Fox, R. O., A CFD model for biomass fast pyrolysis in fluidized-bed reactors. *Chemical Engineering Science* **2011,** *66* (11), 2440-2452 (https://doi.org/10.1016/j.ces.2011.03.010).
8. Xue, Q.; Dalluge, D.; Heindel, T. J.; Fox, R. O.; Brown, R. C., Experimental validation and CFD modeling study of biomass fast pyrolysis in fluidized-bed reactors. *Fuel* **2012,** *97*, 757-769 (https://doi.org/10.1016/j.fuel.2012.02.065).
9. Bruchmüller, J.; van Wachem, B. G. M.; Gu, S.; Luo, K. H.; Brown, R. C., Modeling the thermochemical degradation of biomass inside a fast pyrolysis fluidized bed reactor. *AIChE Journal* **2012,** *58* (10), 3030-3042 (https://doi.org/10.1002/aic.13705).
10. Xue, Q.; Fox, R. O., Computational Modeling of Biomass Thermochemical Conversion in Fluidized Beds: Particle Density Variation and Size Distribution. *Industrial & Engineering Chemistry Research* **2015,** *54* (16), 4084-4094 (https://doi.org/10.1021/ie503806p).
11. Dong, N. H.; Luo, K. H.; Wang, Q., Modeling of biomass pyrolysis in a bubbling fluidized bed reactor: Impact of intra-particle heat conduction. *Fuel Processing Technology* **2017,** *161*, 199-203 (https://doi.org/10.1016/j.fuproc.2016.09.015).
12. Shi, X.; Ronsse, F.; Pieters, J. G., Finite element modeling of intraparticle heterogeneous tar conversion during pyrolysis of woody biomass particles. *Fuel Processing Technology* **2016,** *148*, 302-316 (https://doi.org/10.1016/j.fuproc.2016.03.010).
13. Anca-Couce, A.; Sommersacher, P.; Scharler, R., Online experiments and modelling with a detailed reaction scheme of single particle biomass pyrolysis. *Journal of Analytical and Applied Pyrolysis* **2017,** *127*, 411-425 (https://doi.org/10.1016/j.jaap.2017.07.008).
14. Pecha, M. B.; Ramirez, E.; Wiggins, G. M.; Carpenter, D.; Kappes, B.; Daw, S.; Ciesielski, P. N., Integrated Particle- and Reactor-Scale Simulation of Pine Pyrolysis in a Fluidized Bed. *Energy & Fuels* **2018,** *32* (10), 10683-10694 (https://doi.org/10.1021/acs.energyfuels.8b02309).
15. Sharifzadeh, M.; Sadeqzadeh, M.; Guo, M.; Borhani, T. N.; Murthy Konda, N. V. S. N.; Garcia, M. C.; Wang, L.; Hallett, J.; Shah, N., The multi-scale challenges of biomass fast pyrolysis and bio-oil upgrading: Review of the state of art and future research directions. *Progress in Energy and Combustion Science* **2019,** *71*, 1-80 (https://doi.org/10.1016/j.pecs.2018.10.006).
16. Peters, J. F.; Banks, S. W.; Bridgwater, A. V.; Dufour, J., A kinetic reaction model for biomass pyrolysis processes in Aspen Plus. *Applied Energy* **2017,** *188*, 595-603 (https://doi.org/10.1016/j.apenergy.2016.12.030).
17. Ranzi, E.; Debiagi, P. E. A.; Frassoldati, A., Mathematical Modeling of Fast Biomass Pyrolysis and Bio-Oil Formation. Note I: Kinetic Mechanism of Biomass Pyrolysis. *ACS Sustainable Chemistry & Engineering* **2017,** *5* (4), 2867-2881 (https://doi.org/10.1021/acssuschemeng.6b03096).
18. Kunii, D.; Levenspiel, O., *Fluidization Engineering*. 2nd ed.; Butterworth-Heinemann: Stoneham, MA, 1991.

19. Caudle, B. H.; Gorensek, M. B.; Chen, C.-C., A rigorous process modeling methodology for biomass fast pyrolysis with an entrained-flow reactor. *Journal of Advanced Manufacturing and Processing* **2020,** *2* (1), e10031 (https://doi.org/10.1002/amp2.10031).
20. Brown, R. C., Department of Mechanical Engineering, Iowa State University, Ames, IA. Personal communication. 2019.
21. Polin, J. P.; Peterson, C. A.; Whitmer, L. E.; Smith, R. G.; Brown, R. C., Process intensification of biomass fast pyrolysis through autothermal operation of a fluidized bed reactor. *Applied Energy* **2019,** *249*, 276-285 (https://doi.org/10.1016/j.apenergy.2019.04.154).
22. Gorensek, M. B.; Shukre, R.; Chen, C.-C., Development of a Thermophysical Properties Model for Flowsheet Simulation of Biomass Pyrolysis Processes. *ACS Sustainable Chemistry & Engineering* **2019,** *7* (9), 9017-9027 (https://doi.org/10.1021/acssuschemeng.9b01278).
23. Polin, J. P.; Carr, H. D.; Whitmer, L. E.; Smith, R. G.; Brown, R. C., Conventional and autothermal pyrolysis of corn stover: Overcoming the processing challenges of high-ash agricultural residues. *Journal of Analytical and Applied Pyrolysis* **2019,** *143*, 104679 (https://doi.org/10.1016/j.jaap.2019.104679).
24. Debiagi, P. E. A.; Pecchi, C.; Gentile, G.; Frassoldati, A.; Cuoci, A.; Faravelli, T.; Ranzi, E., Extractives Extend the Applicability of Multistep Kinetic Scheme of Biomass Pyrolysis. *Energy & Fuels* **2015,** *29* (10), 6544-6555 (https://doi.org/10.1021/acs.energyfuels.5b01753).
25. Daugaard, D. E.; Brown, R. C., Enthalpy for Pyrolysis for Several Types of Biomass. *Energy & Fuels* **2003,** *17* (4), 934-939 (https://doi.org/10.1021/ef020260x).
26. Yang, H.; Kudo, S.; Kuo, H.-P.; Norinaga, K.; Mori, A.; Mašek, O.; Hayashi, J.-i., Estimation of Enthalpy of Bio-Oil Vapor and Heat Required for Pyrolysis of Biomass. *Energy & Fuels* **2013,** *27* (5), 2675-2686 (https://doi.org/10.1021/ef400199z).
27. Ranzi, E.; Debiagi, P. E. A.; Frassoldati, A., Mathematical Modeling of Fast Biomass Pyrolysis and Bio-Oil Formation. Note II: Secondary Gas-Phase Reactions and Bio-Oil Formation. *ACS Sustainable Chemistry & Engineering* **2017,** *5* (4), 2882-2896 (https://doi.org/10.1021/acssuschemeng.6b03098).
28. Humbird, D.; Trendewicz, A.; Braun, R.; Dutta, A., One-Dimensional Biomass Fast Pyrolysis Model with Reaction Kinetics Integrated in an Aspen Plus Biorefinery Process Model. *ACS Sustainable Chemistry & Engineering* **2017,** *5* (3), 2463-2470 (https://doi.org/10.1021/acssuschemeng.6b02809).

FOR TABLE OF CONTENTS USE ONLY

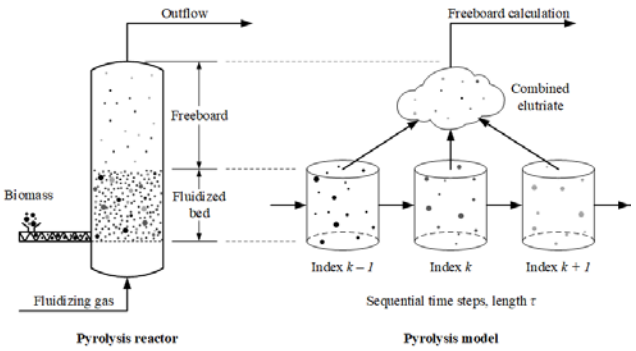

Biomass pyrolysis in a fluidized bed is modeled using a commercial simulator to capture all process fundamentals and performance metrics.

Supporting Information

for

A novel approach to modeling biomass pyrolysis in a fluidized bed reactor

Benjamin H. Caudle[†], Maximilian B. Gorensek[‡,*], Chau-Chyun Chen[†]

[†]Department of Chemical Engineering, Texas Tech University, PO Box 43121, Lubbock, TX 79409-3121

[‡]Advanced Modeling, Simulation, and Analytics, Savannah River National Laboratory, Savannah River Site, 703-41A/225, Aiken, SC 29808

[*]Phone: +1 803 725-1314. E-mail: maximilian.gorensek@srnl.doe.gov.

8 pages, 1 figure, 2 tables, 1 nomenclature list, 1 reference list

Derivation of biomass surface area

While the exact surface area of the biomass particles has a negligible contribution to the results of the fluidized bed pyrolysis reactor, it is important to have an order-of-magnitude estimation of the value in order to yield accurate overall results. The area estimation begins with the total volume of biomass in the k^{th} time step, $V_{b,k}$ (m^3), using the total biomass flow rate, time step length, and biomass density:

$$V_k = \frac{\dot{M}_k \tau}{\rho_{b,k}} \tag{S-1}$$

Assuming that the biomass particles can be represented as spheres, the number of biomass particles, n_k depends on the total volume and the volume of each sphere:

$$n_k = \frac{V_k}{\frac{4}{3}\pi r_{p,k}^3} \tag{S-2}$$

The surface area of a single particle $a_{p,k}$ (m^2) is taken from the mean particle radius:

$$a_{p,k} = 4\pi r_{p,k}^2 \tag{S-3}$$

Combining equations (S-1) through (S-3) yields an expression for estimating the biomass heat transfer area of each time step, a_k:

$$a_k = n_k a_{p,k} = \frac{3}{4}\left(\frac{\dot{M}_k \tau}{\rho_{b,k}\pi\, r_{p,k}^3}\right) 4\pi r_{p,k}^2 = \frac{6\dot{M}_k \tau}{\rho_{b,k} d_{p.k}} \tag{S-4}$$

Chemical species used in biomass pyrolysis process model

Table S-1 Chemical species used in biomass pyrolysis process model.[1]

Chemical compound	Component ID	Type[a]	Component name[b]	Formula
Biomass components:				
Tannin	TANN	Solid		$C_{15}H_{12}O_7$
C-rich lignin	LIGC	Solid		$C_{15}H_{14}O_4$
O-rich lignin	LIGO	Solid		$C_{20}H_{22}O_{10}$
H-rich lignin	LIGH	Solid		$C_{22}H_{28}O_9$
Triglyceride	TGL	Conventional		$C_{57}H_{100}O_7$
Hemicellulose-glucomannan	GMSW	Solid		$C_5H_8O_4$
Hemicellulose-xylan	XYHW	Solid		$C_5H_8O_4$
Cellulose	CELL	Solid		$C_6H_{10}O_5$
Ash	ASH	Solid	CALCIUM-OXIDE	CaO
Moisture	H2OL	Conventional	WATER	H_2O
Biomass pyrolysis intermediate species:				
Secondary lignin intermediate	LIG	Solid		$C_{11}H_{12}O_4$
C-rich lignin intermediate	LIGCC	Solid		$C_{15}H_{14}O_4$
H/O-rich lignin intermediate	LIGOH	Solid		$C_{19}H_{22}O_8$
Activated hemicellulose 1	HCE1	Solid		$C_5H_8O_4$
Activated hemicellulose 2	HCE2	Solid		$C_5H_8O_4$
Activated cellulose	CELLA	Solid		$C_6H_{10}O_5$
Tannin intermediate	ITANN	Solid		$C_8H_4O_4$
Biomass pyrolysis end products:				
Char	CHAR	Solid	CARBON-GRAPHITE	C
Sinapyl aldehyde	FE2MACR	Conventional		$C_{11}H_{12}O_4$
Free fatty acid	FFA	Conventional	LINOLEIC-ACID	$C_{18}H_{32}O_2$
High-molecular weight lignin	HMWL	Solid		$C_{24}H_{28}O_4$
Glyoxal	GLYOX	Conventional	GLYOXAL	$C_2H_2O_2$
Ethylene	C2H4	Conventional	ETHYLENE	C_2H_4
Acetaldehyde	CH3CHO	Conventional	ACETALDEHYDE	C_2H_4O
Acetic acid	ACAC	Conventional	ACETIC-ACID	$C_2H_4O_2$
Glycol aldehyde	HAA	Conventional	GLYCOL-ALDEHYDE	$C_2H_4O_2$
Ethanol	C2H5OH	Conventional	ETHANOL	C_2H_6O
Acrolein	ACROL	Conventional	ACROLEIN	C_3H_4O
n-Propionaldehyde	ALD3	Conventional	N-PROPIONALDEHYDE	C_3H_6O
3-Hydroxypropanal	C3H6O2	Conventional		$C_3H_6O_2$

[a] "Conventional" species participate in vapor-liquid equilibrium, while "solid" species do not.
[b] Component name in aspenONE databank.

Chemical compound	**Component ID**	**Type**[a]	**Component name**[b]	**Formula**
Furfural	FURF	Conventional	FURFURAL	$C_5H_4O_2$
Xylosan	XYLAN	Conventional		$C_5H_8O_4$
Levoglucosan	LVG	Conventional	LEVOGLUCOSAN	$C_6H_{10}O_5$
Phenol	PHENOL	Conventional	PHENOL	C_6H_6O
5-Hydroxymethyl-furfural	HMFU	Conventional	5-HYDROXY-METHYLFURFURAL	$C_6H_6O_3$
Anisole	ANISOLE	Conventional	METHYL-PHENYL-ETHER	C_7H_8O
p-Coumaryl alcohol	COUMARYL	Conventional		$C_9H_{10}O_2$
Formaldehyde	CH2O	Conventional	FORMALDEHYDE	CH_2O
Formic acid	HCOOH	Conventional	FORMIC-ACID	CH_2O_2
Methane	CH4	Conventional	METHANE	CH_4
Methanol	CH3OH	Conventional	METHANOL	CH_4O
Carbon monoxide	CO	Conventional	CARBON-MONOXIDE	CO
Carbon dioxide	CO2	Conventional	CARBON-DIOXIDE	CO_2
Hydrogen	H2	Conventional	HYDROGEN	H_2
Water	H2O	Conventional	WATER	H_2O
Non-biomass components:				
Argon	AR	Conventional	ARGON	Ar
Nitrogen	N2	Conventional	NITROGEN	N_2
Oxygen	O2	Conventional	OXYGEN	O_2
Sand	SAND	Solid	SILICON-DIOXIDE	SiO_2

Pyrolysis reactions and kinetics used in reactor model

Table S-2 Biomass pyrolysis reaction mechanism from Caudle et al.,[2] adapted from Ranzi et al. (I),[3] (compound names defined by Gorensek et al.[1]).

Reaction No., *n*	**Reaction**	A_n [$K^{-x_n} \cdot s^{-1}$]	x_n	E_n [kcal/kmol]
1	CELL → CELLA	1.5×10^{14}	0	47000
2	CELLA → 0.4 HAA + 0.05 GLYOX + 0.15 CH3CHO + 0.25 HMFU + 0.35 ALD3 + 0.15 CH3OH + 0.3 CH2O + 0.61 CO + 0.36 CO2 + 0.25 H2 + 0.93 H2O + 0.02 HCOOH + 0.05 C3H6O2 + 0.05 CH4 + 0.61 CHAR	2.5×10^{6}	0	19100
3	CELLA → LVG	3.3	1	10000
4	CELL → 5 H2O + 6 CHAR	6×10^{7}	0	31000
5	GMSW → 0.7 HCE1 + 0.3 HCE2	1×10^{10}	0	31000
6	XYHW → 0.35 HCE1 + 0.65 HCE2	1×10^{10}	0	28500
7	HCE1 → 0.6 XYLAN + 0.2 C3H6O2 + 0.12 GLYOX + 0.2 FURF + 0.4 H2O + 0.08 H2 + 0.16 CO	3	1	11000
8	HCE1 → 0.4 H2O + 0.8 CO2 + 0.05 HCOOH + 1.6 CO + 1.25 H2 + 0.3 CH2O + 0.625 CH4 + 0.375 C2H4 + 0.875 CHAR	1.8×10^{-3}	1	3000
9	HCE2 → 0.2 H2O + CO + 0.575 CO2 + 0.4 CH2O + 0.1 C2H5OH + 0.05 HAA + 0.35 ACAC + 0.025 HCOOH + 0.25 CH4 + 0.3 CH3OH + 0.225 C2H4 + 0.725 H2 + CHAR	5×10^{9}	0	31500
10	LIGC → 0.35 LIGCC + 0.1 COUMARYL + 0.08 PHENOL + 0.41 C2H4 + H2O + 1.02 CO + 0.7 H2 + 0.3 CH2O + 0.495 CH4 + 5.735 CHAR	1×10^{11}	0	37200
11	LIGH → LIGOH + 0.5 ALD3 + 0.5 C2H4 + 0.2 HAA + 0.1 CO + 0.1 H2	6.7×10^{12}	0	37500
12	LIGO → LIGOH + CO2	3.3×10^{8}	0	25500
13	LIGCC → 0.3 COUMARYL + 0.2 PHENOL + 0.35 HAA + 0.7 H2O + 0.65 CH4 + 0.6 C2H4 + H2 + 1.8 CO + 6.75 CHAR	1×10^{4}	0	24800
14	LIGOH → 0.9 LIG + H2O + 0.45 CH4 + 0.9 CH3OH + 0.9 H2 + 0.05 CO2 + 2.1 CO + 0.05 HCOOH + 0.2 C2H4 + 0.025 HMWL + 0.1 ACROL + 4.25 CHAR	1×10^{8}	0	30000
15	LIG → 0.7 FE2MACR + 0.3 ANISOLE + 0.6 CO + 0.3 CH3CHO	4	1	12000
16	LIG → 0.6 H2O + 2.6 CO + 0.6 CH4 + 0.4 CH2O + 0.5 C2H4 + 0.4 CH3OH + 2 H2 + 6 CHAR	8.3×10^{-2}	1	8000
17	LIG → 0.6 H2O + 2.6 CO + 1.1 CH4 + 0.4 CH2O + C2H4 + 0.4 CH3OH + 4.5 CHAR	1×10^{7}	0	24300
18	TGL → ACROL + 3 FFA	7×10^{12}	0	45700
19	TANN → PHENOL + CO + H2O + ITANN	20	0	10000
20	ITANN → 5 CHAR + 3 CO + H2O + H2	1×10^{3}	0	25000
21	H2O → H2OL	1	1	8000

Biomass Particle Size Distribution

The particle size distribution of Red Oak was measured by Polin et al.[4] and given the continuous density functions shown in the figure (below).

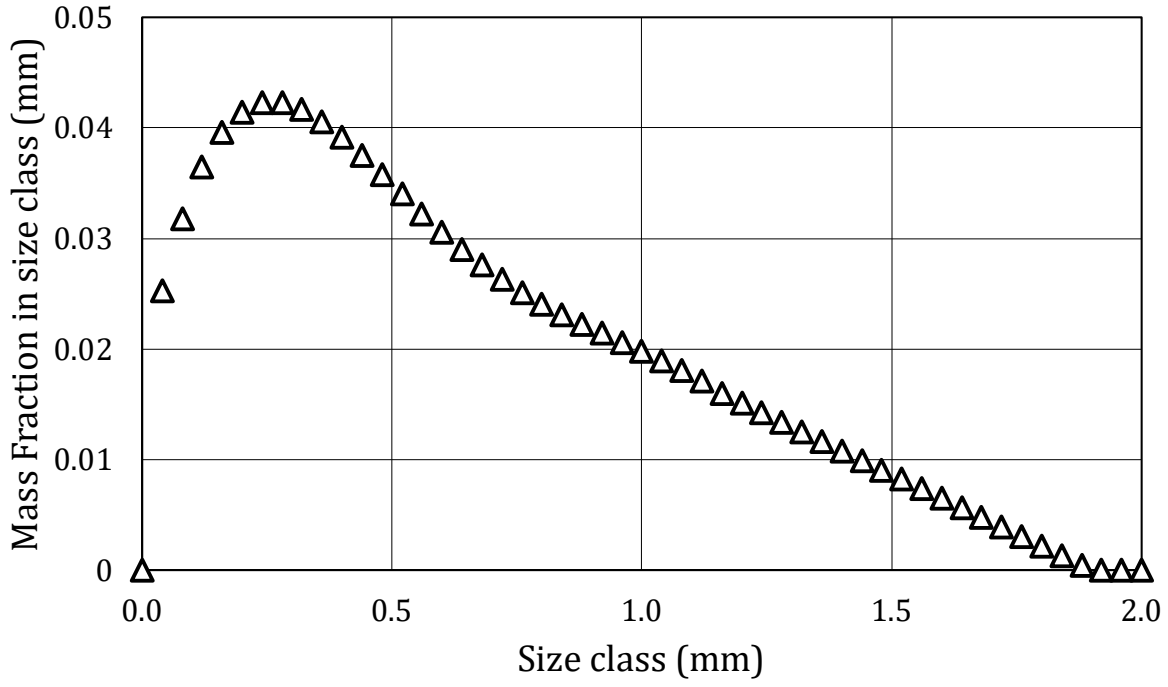

Figure S-1 Particle size distribution for red oak provided by Polin et al.[4]

Nomenclature

Symbol	Description	Units
	Latin symbols	
A_n	Reaction n rate constant pre-exponential coefficient	$K^{-x_n} \cdot s^{-1}$
a_k	Heat transfer area as biomass passes through k^{th} time step	m^2
$a_{p,k}$	Surface area of single particle in k^{th} time step	m^2
B	Empirical constant in ash factor catalytic activity adjustment	kcal/kmol
$C_{P,g}$	Fluidizing gas heat capacity	kJ/kg-K
$C_{P,k}$	Biomass heat capacity entering k^{th} time step	kJ/kg-K
d_j	Characteristic particle diameter for size class j	m
$d_{p,k}$	Biomass particle mass-weighted mean diameter entering k^{th} time step (calculated from PSD)	m
$d^*_{j,k}$	Dimensionless particle diameter for solids in size class j for k^{th} time step	–
E_n	Activation energy of n^{th} reaction	kcal/kmol

Symbol	Description	Units
E_n^0	Activation energy of n^{th} reaction in the absence of ash catalytic activity	kcal/kmol
F	Empirical factor in heat transfer correlation	–
F_a	Biomass-specific factor to account for catalytic activity of ash	–
$f_{j,k}$	Mass fraction of particles of size class *j* entering time step *k*	–
g	Acceleration due to gravity	m/s^2
$h_{p,k}$	Convective heat transfer coefficient (fluidized bed to biomass) over k^{th} time step	kJ/m^2-s-K
k_g	Fluidizing gas thermal conductivity	kJ/m-s-K
L_B	Height of fluidized bed	m
$\dot{M}_k$	Biomass mass flow rate entering k^{th} time step	kg/s
$\dot{m}_{j,k}^e$	Mass flow rate of biomass particles in j^{th} size class (after reaction) before elutriation in k^{th} step	kg/s
$\dot{m}_{i,k}$	Mass flow rate of biomass component *i* entering k^{th} step	kg/s
$\dot{m}_{n,k}$	Mass flow rate of biomass reactant consumed in n^{th} reaction entering k^{th} step	kg/s
n_k	Total number of biomass particles in k^{th} time step	–
Nu_k	Nusselt number for gas-solid heat transfer over k^{th} time step	–
pct_{ash}	Mass percent of ash in the biomass	mass-%
Pr	Prandtl number of fluidizing gas	–
$\dot{q}_{a,k}$	Heat absorption rate due to biomass sensible heat over k^{th} time step	kJ/s
$\dot{q}_{r,k}$	Heat consumption rate due to biomass pyrolysis reactions over k^{th} time step	kJ/s
$\dot{q}_{t,k}$	Convective heat transfer rate from fluidized bed to biomass over k^{th} time step	kJ/s
R_C	Universal gas constant	kcal/kmol-K
$r_{n,k}$	Rate of n^{th} reaction at temperature of k^{th} time step	kg/s
$r_{p,k}$	Biomass particle mean radius entering k^{th} time step	m
$\mathrm{Re}_{p,k}$	Biomass particle Reynolds number entering k^{th} time step	–
T_B	Fluidized bed temperature	K
T_k	Biomass temperature entering k^{th} time step	K
u_0	Fluidizing gas superficial velocity	m/s
$u_{j,k}^t$	Terminal velocity for solids in size class *j* for k^{th} time step	m/s
$u_{j,k}^*$	Dimensionless terminal velocity for solids in size class *j* for k^{th} time step	–
$V_{b,k}$	Total volume of biomass in k^{th} time step	m^3
W_i	Molecular weight of i^{th} component	kg/kmol
W_n	Molecular weight of reactant in n^{th} pyrolysis reaction	kg/kmol
x_n	Reaction *n* rate constant pre-exponential temperature exponent	–

Symbol	Description	Units
	Greek symbols	
$\Delta h_{i,k}^{f}$	Heat of formation of i^{th} component at temperature and pressure of k^{th} time step	kJ/kg
$\Delta \dot{M}_{k}^{r}$	Change in total biomass flow rate over time step k due to volatilization	kg/s
$\Delta \dot{m}_{i,k}^{e}$	Mass flow rate change due to elutriation of biomass component i over time step k	kg/s
$\Delta \dot{m}_{j,k}^{e}$	Mass flow rate change due to elutriation of biomass particles in size class j over time step k	kg/s
$\Delta \dot{m}_{i,k}^{r}$	Mass flow rate change due to reaction of i^{th} component over k^{th} time step	kg/s
ϵ_B	Fluidized bed void fraction	–
$K_{j,k}$	General elutriation rate constant for solids in size class j and time step k	kg/m^2-s
$\kappa_{j,k}$	Elutriation rate constant for solids in size class j and time step k	s^{-1}
μ_g	Fluidizing gas viscosity	Pa-s
ν_g	Fluidizing gas kinematic viscosity	m^2/s
$\nu_{i,n}$	Stoichiometric coefficient of component i in reaction n (negative for reactants, positive for products)	–
$\rho_{b,k}$	Biomass density entering k^{th} time step	kg/m^3
ρ_g	Density of fluidizing gas at bed surface	kg/m^3
τ	Length of each individual time step	s
Ψ	Sphericity of biomass particles	–
	Subscripts	
b	Biomass	
g	Fluidizing gas phase	
i	Component identification	
j	Size class identification	
k	Time step identification	
n	Pyrolysis reaction identification	
p	(Biomass) particle	
0	Inlet condition	

References

1. Gorensek, M. B.; Shukre, R.; Chen, C.-C., Development of a Thermophysical Properties Model for Flowsheet Simulation of Biomass Pyrolysis Processes. *ACS Sustainable Chemistry & Engineering* **2019,** *7* (9), 9017-9027.
2. Caudle, B. H.; Gorensek, M. B.; Chen, C.-C., A rigorous process modeling methodology for biomass fast pyrolysis with an entrained-flow reactor. *Journal of Advanced Manufacturing and Processing* **2020,** *2* (1), e10031.
3. Ranzi, E.; Debiagi, P. E. A.; Frassoldati, A., Mathematical Modeling of Fast Biomass Pyrolysis and Bio-Oil Formation. Note I: Kinetic Mechanism of Biomass Pyrolysis. *ACS Sustainable Chemistry & Engineering* **2017,** *5* (4), 2867-2881.
4. Polin, J. P.; Peterson, C. A.; Whitmer, L. E.; Smith, R. G.; Brown, R. C., Process intensification of biomass fast pyrolysis through autothermal operation of a fluidized bed reactor. *Applied Energy* **2019,** *249*, 276-285.